Characterization of viscoelastic media combining ultrasound and magnetic-force induced vibrations on an embedded ferromagnetic sphere

Alejandro Cebrecos, Noé Jiménez, *Member, IEEE*, Rafael Tarazona, Miguel Company, José María Benlloch and Francisco Camarena

***Abstract*—We report a method to locally assess the complex shear modulus of a viscoelastic medium. The proposed approach is based on the application of a magnetic force to a ferromagnetic sphere embedded in the medium and the subsequent monitoring of its dynamical response. A coil is used to create a magnetic field inducing the displacement of the ferromagnetic sphere located inside a gelatin phantom. Then, a phased-array system using 3 MHz ultrasound probe operating in pulse-echo mode is used to track the displacement of the sphere. Experiments were conducted on several samples and repeated as a function of phantom temperature. The dynamical response of the sphere measured experimentally is in good agreement with Kelvin-Voigt theory. The estimated viscoelastic parameters show excellent robustness and agree the measurements using a quasi-static indentation method, obtaining errors below 10% in the whole temperature range. Since the magnetic force is not affected by weak diamagnetic media, our proposal results in an accurate estimation of the force acting on the inclusion. Consequently, it increases the robustness on the estimation of the viscoelastic parameters of the surrounding medium.**

***Index Terms*—Ultrasound, Magneto-motive, Shear Modulus; Viscoelasticity; Magnetic force**

I. Introduction

THE assessment of the mechanical properties of viscoelastic media is of great interest in medicine, where biomechanical properties of tissue have been proved to be often correlated with their physiological state [1]–[3], and in industry, where the knowledge of the mechanical properties of the medium allows to predict the properties, appearance, processing, and performance of polymers [4], [5], concrete [6], [7], asphalt [8] or food [9], [10].

The mechanical response of a solid sphere subjected to the effect of an external force can be used to determine the viscoelastic properties of the surrounding medium. This relation was first explored theoretically by Oestreicher considering a Kelvin-Voigt rheological model in a medium with equal stiffness and viscosity [11]. Later, Ilinskii *et al.* obtained the static and transient displacement responses of a sphere and a bubble embedded in an elastic medium [12], and Aglyamov et al. extended the work to viscoelastic media [13]. Finally, in 2011, Urban *et al.* proposed a theoretical development to describe the generalized embedded sphere response both in time and frequency domains so that any viscoelastic rheological model can be used [14].

From these theoretical works, several studies have been carried out to locally characterize tissue-like phantoms by exciting a sphere within the acoustic radiation force (ARF) produced at the focus of an ultrasonic beam. The group of Prof. Greenleaf presented a quantitative model for a sphere vibrated by two ultrasound beams of nearby frequencies able to estimate the material properties of the medium surrounding a sphere [15]. Later, the group of Prof. Emelianov locally assessed the shear modulus of a medium by using the ARF generated at the focus of a focused ultrasound beam excited with a short pulse [16]. In addition, the motion of the media due to magnetomotive-generated shear waves can also be measured [17], but to our knowledge this method has not been applied to estimate the viscoelastic parameters of the medium.

In this paper we propose a new method to estimate the viscoelastic parameters of soft-solids. We use a classical Magneto-Motive Ultrasound (MMUS) experimental setup [18]–[22] to track the dynamics of a macroscopic ferromagnetic sphere embedded in a gelatin phantom excited by an external magnetic force, as sketched in Fig. 1. First, a coil is excited with an electrical pulse. Second, the generated magnetic field produces a transient attracting force on the ferromagnetic inclusion. Third, using a 64-channel phased-array system, the position of the inclusion is dynamically tracked, and by using cross-correlation methods the time-

Date: July 14, 2021. This research has been supported by the Spanish Ministry of Science, Innovation and Universities through grant “Juan de la Cierva - Incorporación” (IJC2018-037897-I), and program “Proyectos I+D+i 2019” (PID2019-111436RB-C22), by the Agència Valenciana de la Innovació through grant INNCON/2021/8 and by Generalitat Valenciana through grant AICO/2020/268. Action co-financed by the European Union through the Programa Operativo del Fondo Europeo de Desarrollo Regional (FEDER) of the Comunitat Valenciana 2014-2020 (IDIFEDER/2018/022). A.C. received financial support from Universitat Politècnica de València through program PAID-10-19.

A. Cebrecos, N. Jiménez, R. Tarazona, M. Company, J. M. Benlloch and F. Camarena are with the Instituto de Instrumentación para Imagen Molecular, Universitat Politècnica de València, Consejo Superior de Investigaciones Científicas, València, 46022 Spain (e-mail: nojigon@upv.es).

varying displacement waveform of the sphere is obtained. Finally, the elastic parameters of the surrounding viscoelastic medium are estimated from the dynamics of the sphere.

The procedure is similar to the one used in previous works that make use of ARF [15], [16], but in this case we use a magnetic force acting on a ferromagnetic inclusion. A common problem in ARF-based techniques is that it is difficult to accurately measure or estimate the magnitude of the applied force. This is mainly caused because ultrasound waves attenuate as they propagate into heterogeneous tissues, the magnitude of the ARF depends on the geometry and properties of the object itself and tissue absorption, and in addition weakly nonlinear effects can be relevant into the estimation of the ARF. The uncertainty in the estimation of the ARF directly has an impact on the accuracy of the estimated viscoelastic parameters. In contrast, since the magnetic force is almost not affected by tissues which are, in general, weak diamagnetic media, our proposal results in an accurate estimation of the force acting on the sphere. In addition, ARF should induce motion not only at the bead, but on the viscoelastic media due to ultrasound attenuation and scattering at heterogeneities. Using a magnetic force, only the sphere is pulled. Therefore, it increases the robustness on the estimation of the viscoelastic parameters of the surrounding medium.

It is important to remark that while the setup is similar to MMUS techniques that track the motion of a soft-solid produced by magnetic nanoparticles [18]–[22], we make use of a millimetre-size ferromagnetic sphere. As we will demonstrate, the use of this inclusion allows an accurate estimation of the force exerted on it, enabling the quantitative estimation of the viscoelastic parameters.

The paper is structured as follows: Section II presents the theoretical model to describe the dynamics of a solid sphere embedded in a viscoelastic medium and to evaluate the magnetic force on the sphere. Section III shows the experimental setup and methods. Section IV provides the experimental results and their comparison using indentation techniques. Finally, the concluding remarks are given in Sec. V.

II. Model

A. Dynamics of a solid sphere embedded in viscoelastic media

The bulk modulus of most soft-tissues and tissue phantoms is several orders of magnitude higher than their shear moduli. Therefore, to model low-frequency shear deformations these media can be considered incompressible viscoelastic medium, whose equations of motion for a Kelvin-Voigt-type medium are given by [13]:

$$\rho \frac{\partial^2 \mathbf{u}}{\partial t^2} = -\nabla p + \mu \nabla^2 \mathbf{u} + \eta \nabla^2 \frac{\partial \mathbf{u}}{\partial t}, \tag{1}$$

where $\mathbf{u} = \mathbf{u}(t, \mathbf{r})$ is the displacement vector, $p = p(\mathbf{r})$ is the internal pressure, μ and η are the shear elastic and shear viscous coefficients, ρ is the density of the medium and t is the time. Assuming a Fourier convention of $e^{-i\omega t}$, the equations of motion in the frequency domain are written as

$$-\nabla P + G \nabla^2 \mathbf{U} + \rho \omega^2 \mathbf{U} = 0, \tag{2}$$

where P and $\mathbf{U}$ are the Fourier transforms of p and $\mathbf{u}$, ω is the angular frequency and $G = (\mu - i\omega\eta)$ is the complex shear modulus. We consider a rigid sphere embedded in the viscoelastic medium submitted to a transient external force $F_z^{\mathrm{ext}}(t)$, acting on direction z. In the frequency domain, and for small displacements, the z component of the displacement of the sphere $U_z(\omega)$ and the Fourier transform of the external force $F_z^{\mathrm{ext}}(\omega)$ are linearly related by [12]:

$$F_z^{\mathrm{ext}}(\omega) = \left[-M\omega^2 + 6\pi G R \left(1 - ikR - \frac{1}{9} k^2 R^2 \right) \right] U_z(\omega), \tag{3}$$

where $M = 4\pi \rho_s R^3/3$ is the mass, ρ_s the density and R is the radius of the solid sphere, and k is the complex wave number in the viscoelastic medium given by the dispersion relation $k^2 = \rho\omega^2/(\mu - i\omega\eta)$. Then, the displacement of the sphere $u_z(t)$ in time domain can be recovered using the inverse Fourier transform as:

$$u_z(t) = \frac{1}{2\pi} \int_{-\infty}^{\infty} U_z(\omega) \mathrm{e}^{-i\omega t} d\omega. \tag{4}$$

In our study, we submit the sphere to a pulsed magnetic force. In practice, obtaining an ideal rectangular waveform for the current is not possible due to the inductance of the coil. Therefore, we assume that the temporal evolution of the magnetic force is given by a trapezoidal pulse with a finite rise time, as shown in Fig. 1 (c), as

$$F_z^{\mathrm{trap}}(t) = \begin{cases} -F_0 \left(\dfrac{t}{t_r} \right) & 0 \le t \le t_r, \\ -F_0 & t_r \le t \le t_0, \\ -F_0 \left(1 - \dfrac{t - t_0}{t_r} \right) & t_0 \le t \le t_0 + t_r, \\ 0 & t > t_0 + t_r, \end{cases} \tag{5}$$

where t_0 is the pulse duration, F_0 is the amplitude of the pulse and t_r is the rise time. The Fourier transform of the trapezoidal pulsed force results in

$$F_z^{\mathrm{trap}}(\omega) = -\frac{F_0}{t_r \omega^2} \left(e^{i\omega t_0} - 1 \right) \left(e^{i\omega t_r} - 1 \right). \tag{6}$$

Combining Eqs. (3, 6) and applying the inverse Fourier transform (4), the displacement of the solid sphere in a viscoelastic medium is written in the time domain as

$$u_z^{\mathrm{trap}}(t) = -\frac{F_0}{12\pi^2 R t_r} \int_{-\infty}^{\infty} \times \frac{\left(\mathrm{e}^{i\omega t_0} - 1 \right) \left(\mathrm{e}^{i\omega t_r} - 1 \right) \mathrm{e}^{-i\omega t}}{\omega^2 (\mu - i\omega\eta) \left(1 - ikR - k^2 R^2 (1 + 2\beta)/9\right)} d\omega, \tag{7}$$

where $\beta = \rho_s/\rho$ is the normalized density of the sphere with respect to the medium density, in analogy with the expression obtained in Ref. [12] for a rectangular pulsed excitation. Equation (7) is integrated numerically to obtain the theoretical estimation of the displacement of the sphere. Note the displacement of the sphere for a long pulse converge to a constant value [12] of $u_0 = F_0/6\pi\mu R$, as it is shown in the example in normalized scale in Fig.1 (c).

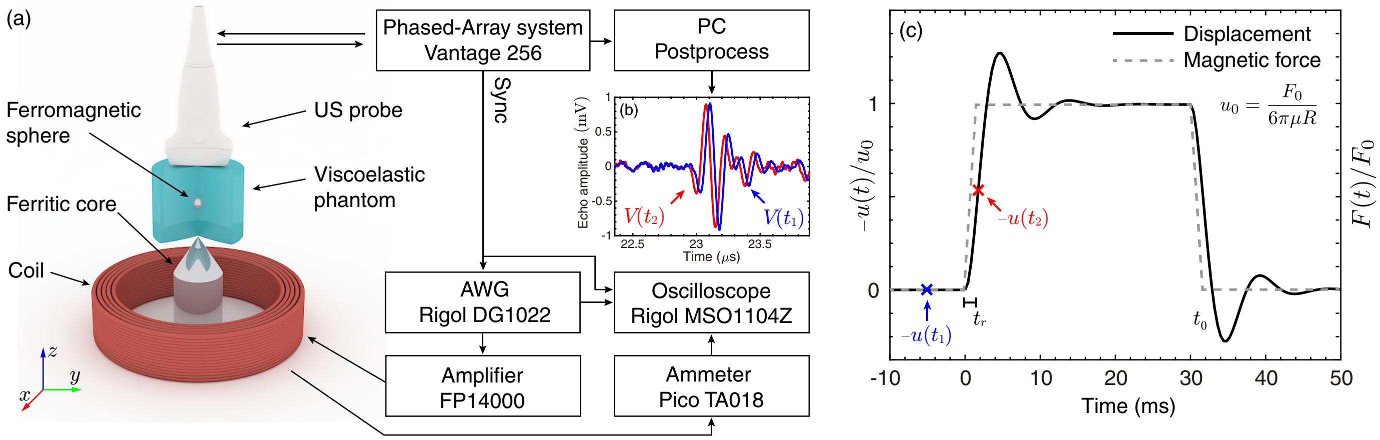

Fig. 1. (a) Sketch and block diagram of the experimental setup. (b) Example of ultrasonic pulse-echo signals: blue line ($\boldsymbol{V(t_1)}$) corresponds to the echo of the sphere at reference position in absence of magnetic force, while red line ($\boldsymbol{V(t_2)}$) corresponds to the echo signal an instant when the magnetic force is present, as indicated in (c) by the colour markers. (c) Magnetic force waveform (dashed line) corresponding to a trapezoidal pulsed excitation of length $\boldsymbol{t_0}$ with a rise time of $\boldsymbol{t_r}$, and expected displacement waveform (continuous line) as a result of the cross-correlation between multiple ultrasonic pulse-echo signals at each time.

B. Magnetic force exerted on the sphere

The magnetic force acting on a small ellipsoid of volume V due to the presence of the magnetic flux density B_0 along the z axis is given by [23]:

$$F_z^{\text{ext}}(z,t) = \frac{\chi V}{\mu_0} B_0(z,t) \frac{\partial B_0(z,t)}{\partial z} \left[\frac{\cos^2\theta}{1+\chi D_a} + \frac{\sin^2\theta}{1+\chi D_r} \right] \tag{8}$$

where χ is the volumetric magnetic susceptibility of the particle, μ_0 is the magnetic permeability in vacuum, D_a is the demagnetizing factor along the axis of symmetry, D_r is the radial demagnetizing factor, and θ is the angle between the symmetry axis of the particle (x direction) and the magnetic field direction (z axis). For a spherical particle, $D_a = D_r = 1/3$, other relations can be found for other geometries [23].

The ferromagnetic sphere used in this experiment is made of a low-alloy chrome steel (AISI 52100), having a relative magnetic permeability $\mu_r > 300$, therefore, the volumetric magnetic susceptibility $\chi \gg 1$, thus, it can be considered as a soft-ferromagnetic material [24]. As such, both coercivity and hysteresis are relatively small and are neglected for this material in our experiment [25]. All measures in this study are performed at relatively low values of magnetic field (maximum around 100 mT), insufficient to saturate the material. Note the magnetic saturation of the sphere can be roughly estimated as around 2 T for a low-alloy steel with less than 2% of chromium [26]. Therefore, and taking into consideration the spherical geometry of the bead aligned with the magnetic field, at the z axis of the axisymmetric system, the force acting in the ferromagnetic sphere of radius R can be reduced to [23]

$$F_z^{\text{ext}}(z,t) = -\frac{4\pi R^3}{\mu_0} B_z(z,t) \frac{\partial B_z(z,t)}{\partial z}. \tag{9}$$

Note that for a soft-ferromagnetic sphere the ratio between the magnetic field strength, $\mathbf{H}$, and the magnetization of the material, $\mathbf{M}$, does not depend on the magnetic properties of the material [27] and is given by $\mathbf{H} = -3\mathbf{M}$, the induced mechanical force is therefore independent of χ. Also note that Eq. (9) can only be applied if the system is axisymmetric, i.e., the sphere must be accurately located at the axis of the ferritic core. To know the magnetic force amplitude as a function of the electrical current on the coil, a finite element method (FEM) simulation of the whole magnetic system was carried on using COMSOL® 5.2 software. Numerical simulations were carried out and the magnetic field was calculated at different distances from the center of the ferritic core for different values of electrical current. A model was obtained by fitting the simulated data to the power law

$$F_0(z, I_0) = I_0^2 \alpha z^{\gamma}, \tag{10}$$

where I_0 is the electrical current on the coil, z is the distance from ferritic core to the sphere, and α and γ are the fitted parameters of the model. This model, as we will show below, was validated using Eq. (9) and experimental measurements of the magnetic field, and direct measurements of the force on a ferromagnetic sphere using a magnetic scale. The model provides a direct estimation of the force acting on the sphere as a function of the electrical current in the coil and the position of the sphere, parameters that can be accurately measured.

III. Experimental methods

The experimental setup that produces the magnetic force on the ferromagnetic sphere is shown in Fig. 1 (a). On the one hand, we use a copper coil (S1013, Solen Inc.) with a height of 45 mm and a radius of 178 mm. Inside the coil is located a ferritic steel core (AISI 430 steel) with a radius of 35 mm. The coil is excited with a 2800 W power amplifier (FP14000) which receives the excitation signal from an arbitrary waveform generator (Rigol DG1022). In particular, we excite the coil with the proper waveforms to create trapezoidal pulses of electrical current in the coil of $t_0 = 30$ ms duration. An ammeter (TA018, Pico Technology) is used to observe the current in the coil and evaluate the quality of the trapezoidal pulse. We measured a rising time of $t_r = 3$ ms. A three-axis Hall magnetometer (THM1176, Metrolab) is used to characterize the magnetic field of the

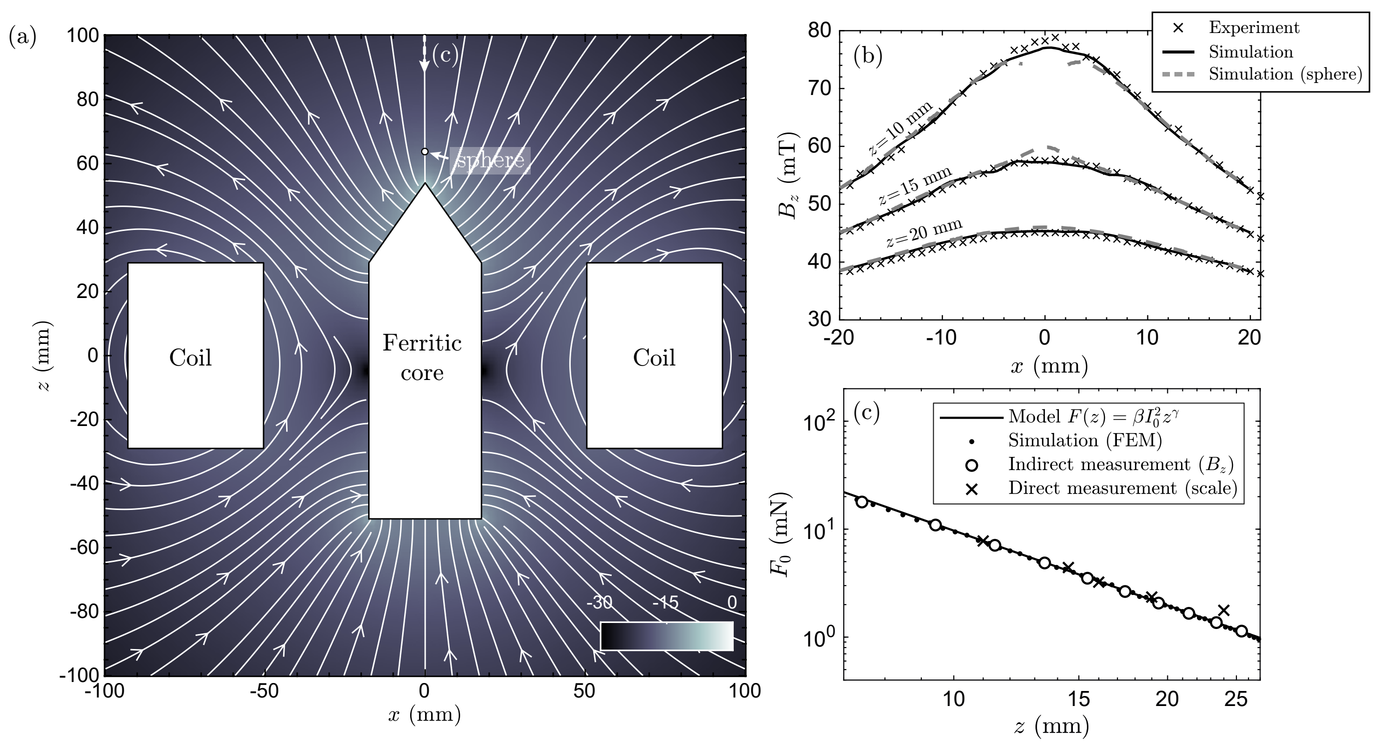

Fig. 2. (a) Scheme of the coil and ferritic core, FEM simulated magnetic flux density, and field lines (white). Colormap in $10\log_{10}|\boldsymbol{B}|/|\boldsymbol{B}|_{\max}$ units. (b) Experimental (markers), simulated (continuous) and simulated including the sphere (dashed-grey) magnetic flux density at heights $z = 10$ mm, $z = 15$ mm and $z = 20$ mm. (c) Magnetic force exerted on the sphere measured experimentally using weighing scale (crosses), calculated from the measured magnetic field (circles), simulated using FEM (dots) and model retrieved using simulated data (continuous line).

system at steady current. The field sensitive volume of the probe is 200 μm $\times$ 200 μm $\times$ 5 μm, the instrument range is up to 3 T with a resolution 0.1 mT, and it provides an accuracy of $\pm 1\%$ T. Finally, a weighing scale (Cent-O-Gram Model 311, OHAUS) is used to experimentally measure the magnetic force exerted on the ferromagnetic sphere (AISI 52100 steel) at different heights in the absence of the viscoelastic medium and under a current of $I_0 = 30$ A. This allows us to validate the force model given by Eq. (9). Note that the magnetic force acting on the sphere depends on the distance to the ferritic core. However, the displacements considered here are smaller than 100 μm and the force presents spatial variations that are below 1%. Therefore, we assume that the magnetic force does not depend on the sphere displacement, only on its position at rest.

The displacement of the sphere is estimated from the temporal shifts of the echoes produced by a phased-array system (Vantage 256, Verasonics) using a 64-channel 3 MHz ultrasound probe (P4-2V, Verasonics) as shown in Figs. 1 (b,c). The phased-array is set to a pulse repetition frequency of 4 kHz, allowing the reception of an echo every 0.25 ms. The radio-frequency (RF) signals from the ultrasound probe are acquired by the phased-array with a total recording duration of 75 ms. The position of the sphere is given by the cross-correlation between the RF signals and a reference signal in which the sphere is at rest, i.e., in its initial state without being magnetically excited [28]. Interpolation up to a sampling frequency of 15.6 GHz is considered here to increase the accuracy on the estimated displacements up to a resolution of 0.1 μm.

We consider 2 different gelatin phantoms of cylindrical shape with a diameter of 30 mm and a volume of 25 ml. First, "phantom A" was produced mixing water and 200 Bloom gelatin powder, with a gelatin concentration of 60 g/l. Second, "phantom B" was produced mixing water, glycerol (99.5% purity) and 200 Bloom gelatin powder, with concentration of 60 g/l and a glycerol concentration of 40% of the total volume. The density of both phantoms was measured independently, obtaining slightly different densities for both phantoms, as expected ($\rho_A = 1010$ kg/m^3, $\rho_B = 1080$ kg/m^3). A 2.000 ± 0.001 mm diameter ferromagnetic sphere of normalized steel (AISI 52100) was introduced during the manufacturing of both phantoms at about 15 mm from the bottom surface. The location of the sphere was measured using pulse-echo measurements.

The measurement procedure is as follows: first, the sample is prepared and located in front of the ferritic core as shown in Fig. 1 (a). Second, the coil is electrically excited and a pulsed magnetic force is generated on the ferromagnetic sphere. Third, the motion of the sphere is tracked by the phased-array system. Finally, the viscoelastic parameters of the medium are obtained by minimization techniques. We use a curve-fitting algorithm to optimize the values of μ and η that minimizes the least-squares error between the experimental displacement waveform and the theoretical one given by Eq. (7). Note that the value of the magnetic force is fixed during the minimization process. This procedure is repeated 3 times in this work for each experiment.

Experiments were carried out at increasing temperature, taking the samples from a refrigerator and letting them to slowly achieve room temperature. Measurements were taken ranging from 16° C to 26° C. Temperature was measured using two thermistor probes (Tinytag Temperature Logger TK 4023). The first thermistor was located inside the phantom at the same height of the sphere on the lateral wall of the sample container, while the second probe was placed on the top surface of the phantom.

Finally, indentation test were performed using a mechanical testing machine calibrated to measure bloom strength of gelatins (TAXTExpress, Texture Technologies Corp., Hamilton, MA). We used a flat-ended cylinder indenter of radius $a = 1/4$ inch, compressing the samples at a rate of 0.5 mm/s. A maximum displacement of 1 mm was set. The shear modulus was calculated by fitting the force, $F(\Delta z)$, to $F(\Delta z) = 8a\mu\Delta z$ where Δz is the indentation depth [29], [30]. Indentation tests were repeated at different temperatures ranging from 20° to 26° C.

IV. Results

A. Magnetic field and force characterization

We start showing the calibration and validation of the magnetic forces acting on the sphere in the absence of viscoelastic medium. First, the simulated magnetic field in the absence of ferromagnetic sphere is shown in Fig. 2 (a). As expected, the magnetic field is highly enhanced near the tip of the ferritic core. Second, a direct measurement of the magnetic field of the system in static regime has been carried out around the area in which the ferromagnetic sphere will be located, feeding the coil using in this case a continuous current of 20 A. The value of the z component of the magnetic field was sampled along 3 horizontal sweeps of 40 mm in length with a 1 mm pitch in x direction, at 10 mm, 15 mm and 20 mm height from the core, as shown in Fig. 2 (b). The experimental data is in excellent agreement with the simulated magnetic flux density. Simulations including the sphere show that the small ferromagnetic bead do not remarkably disturb the field outside the boundaries of the sphere (see dashed grey lines in Fig. 2 (b)). Finally, the magnetic force as a function of the distance to the coil, i.e., at the axis of symmetry, is shown in Fig. 2 (c). First, the magnetic force was estimated using the simulated magnetic field and Eq. (9) as a function of the height. This was repeated for different currents (from 5 A to 50 A), and Eq. (10) was fitted in a least-squares sense to the simulated force distribution in the range 5 mm $< z <$ 25 mm, obtaining the parameters $\alpha = 2.66 \cdot 10^{-10}$ N/A^2 m$^\gamma$ and $\gamma = -2.3$. To validate this model, the magnetic field was experimentally measured along the axial direction from the tip of the core, from 3 mm to 24 mm, and using Eq. (9) the magnetic force was calculated. In addition, the force was directly measured using a weighing scale with an accuracy of 0.01 grams ($\approx$ 0.1 mN). All measurements, direct and indirect, agree with the simulated force, as shown in Fig. 2 (c). The magnitude of the force shows a power-law dependence, decreasing faster near the tip of the ferritic core (note data in Fig. 2 (c) is in a logarithmic scale). For distances around 20

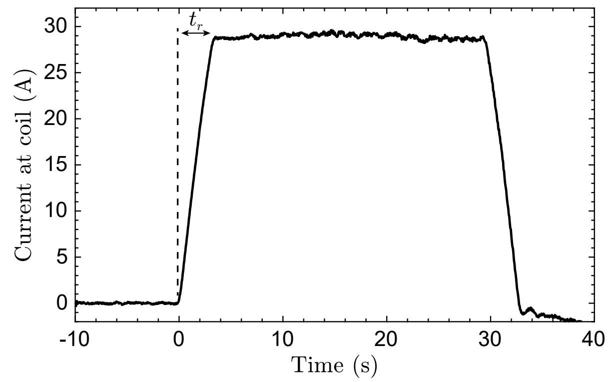

Fig. 3. Experimental electrical pulse (current) as a function of the time. Dashed line marks the rising time, t_r.

mm and for small displacements of the order of 100 μm, force variations are small with respect to the force value (< 1 %). Therefore, we consider constant the magnetic force exerted on the moving sphere around a fixed depth.

For the viscoelastic measurements, the coil was feed with a current pulse of $t_0 = 30$ ms and $I_0 = 30$ A. As the coil presents a finite inductance, the current pulse shows a finite rising time, that for the current setup was set to $t_r = 3$ ms, as measured experimentally, see Fig. 3. As compared with a flat (ideal) rectangular pulse, the effect of a finite rise time is to smooth the displacement waveform, i.e., the peak velocity of the embedded particle is decreased, and the peak amplitude of its oscillation is reduced. However, as long the correct shape is introduced in the model using Eqs. (5-7), the viscoelastic parameters can be retrieved. Also note that if the pulse is long enough a quasi-static displacement value of $u_0 = F_0/6\pi\mu R$ will be also reached using the trapezoidal pulsed force.

B. Estimation of the viscoelastic parameters

For the first experiment, the displacement waveforms corresponding to phantoms A and B are shown in Fig. 4 for $I_0 = 30$ A and $t_0 = 30$ ms. The distance from the tip of the core to the sphere was estimated using ultrasound echo-impulse measurements, obtaining $z_A = 14.6$ mm for phantom A and $z_B = 15.2$ mm for phantom B. This distance was used to calculate the force acting on the sphere using Eq. (10), as given in Table I, and used for the optimization method to calculate the viscoelastic parameters. First, for the phantom A at 24.4° C we obtain $\mu_A = 1862.6 \pm 4.5$ Pa, $\eta_A \approx 0.610 \pm 0.012$ Pa·s. The theoretical curve for the displacement using the retrieved parameters fits the experiments for the first 15 ms, as shown in Fig. 4 (a). The ratio between the initial slope and the amplitude of the first oscillation, as well as its period is properly fitted by the viscoelastic model. When glycerin is introduced in the phantoms, as in phantom B (Fig. 7(b)), the shear modulus is increased. As the viscous modulus is increased, the first oscillation is damped proportionally to the viscous modulus. In addition, the shear elastic modulus also increases. The viscoelastic model correctly fits the experimental data for this case too, showing, at a similar temperature, larger shear modulus and viscous modulus than phantom A

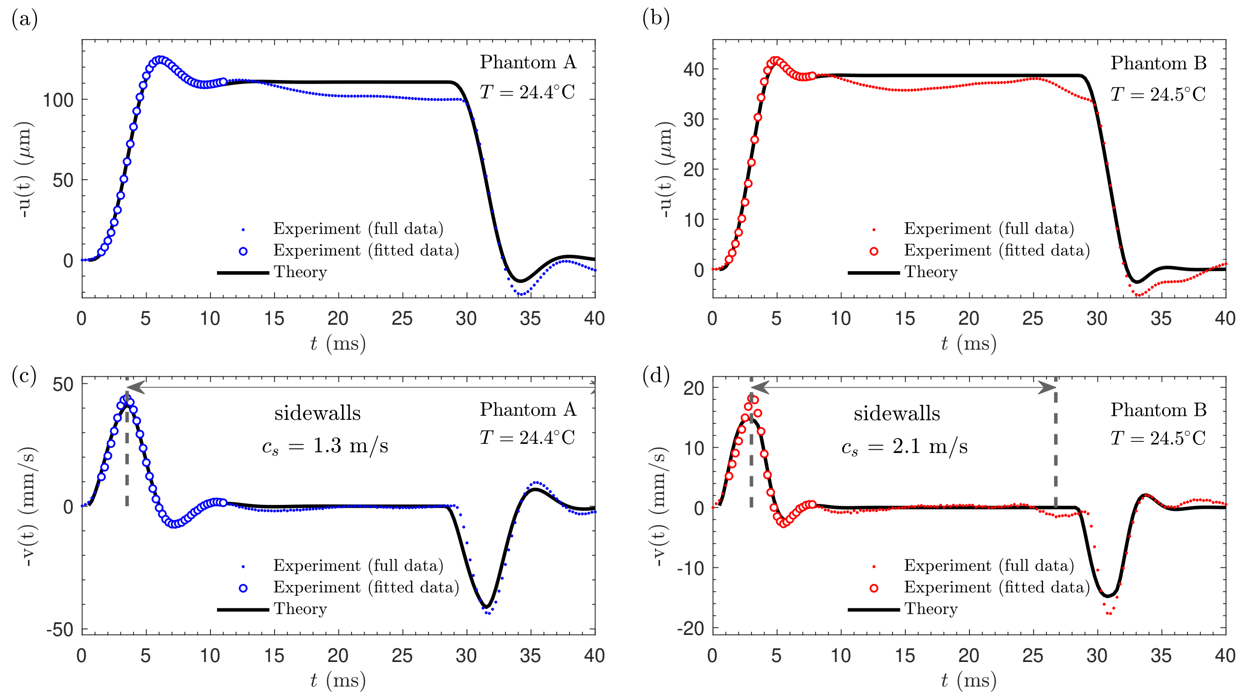

Fig. 4. Dynamics of the sphere embedded in the viscoelastic medium. (a) Displacement waveform for an individual test on the phantom A at $T = 24.4$°C, measured experimentally (circles), using the fitted parameters and the viscoelastic theory (continuous). The data used for fitting was for $t < 8$ ms. (b) Corresponding displacement waveform for the phantom B at $T = 24.5$° C. Velocity waveform calculated from the displacement shown in (a) from experimental displacement data (circles) and using the optimized theoretical expression in Eq. 7 for (c) phantom A and (d) phantom B.

($\mu_B = 4964.4 \pm 25.3$ Pa, $\eta_B = 1.048 \pm 0.034$ Pa·s). The experiment was repeated 3 times and the resulting viscoelastic parameters are listed in Table I. The typical error for the shear elastic modulus is of the order of 2% of the mean value while it is of the order of 10% for the viscous shear modulus. Thus, while the model of the displacement of the sphere is more sensitive to changes in the shear elastic modulus than in the viscous one, the estimation of the shear elastic parameters using the present method shows good repeatability.

It is worth noting here that theory was developed for an infinite medium. However, in practice, when the inclusion is forced to vibrate, shear waves are generated, and they propagate through the finite-size phantom. When shear waves reach the boundaries of the sample they are reflected back and, thus, the vibration of the particle is influenced by them. Figure 4 (c, d) illustrates the velocity signals obtained by taking the derivative of the theoretical and experimental displacement waveforms shown in Figs. 4 (a, b)). In particular, a reflection coming from the sidewalls of the container (located at a distance of $d_w \approx 25$ mm) is observed in Fig. 4(d). By considering the fitted elastic modulus, the shear wave velocity (in the low frequency limit) is $c_{s,B} \approx \sqrt{\mu/\rho} = 2.1$ m/s. The time-of-flight corresponding to the reflection on the sidewalls is shown in grey lines in Fig. 4 (d), and the reflection is visible at the sphere location, validating the calculated shear modulus. On the contrary, the low-frequency limit of the shear wave velocity for phantom A is slower ($c_{s,A} = 1.4$ m/s) and the reflection from the sidewalls arrives when the displacement pulse has already finished (at about $t = 40$ ms). Although one can argue that in this situation the plateau of the experimental displacement pulse should not manifest any deviations from the theoretical one, multiple reflections coming form other boundaries, such as the bottom ($d_b \approx 15$ mm) and top boundaries ($d_t \approx 20$ mm) of the container, prompts a noticeable distortion of the flat part of the pulse. Hence, the time window to the fit was adjusted accordingly in order to capture the dynamical response without shear wave reflections, which, for the conditions of the experiments presented in this work, results in fitting approximately the first 10 ms of the pulse, including the first oscillation. A validation was performed using the indentation tests. For both phantoms, the measured values using the penetrometer agrees the retrieved using the current method, as shown in Table I. Finally, the temperature inside the gelatin was also

TABLE I
ESTIMATED VISCOELASTIC PARAMETERS, AND MEASURED SPHERE LOCATION, MAGNETIC FORCE AND TEMPERATURE.

	Shear elastic modulus		Shear viscous modulus	Sphere position	Magnetic force	Temperature
	Proposed method μ (Pa)	Indentation test μ (Pa)	η (Pa·s)	z (m)	F_0 (mN)	T (°C)
Phantom A	1862.6 ± 4.5	1869.6 ± 11.6	0.610 ± 0.012	14.6	3.922 ± 0.027	24.4
Phantom B	4964.4 ± 25.3	4447.4 ± 13.7	1.048 ± 0.034	15.2	3.623 ± 0.025	24.5

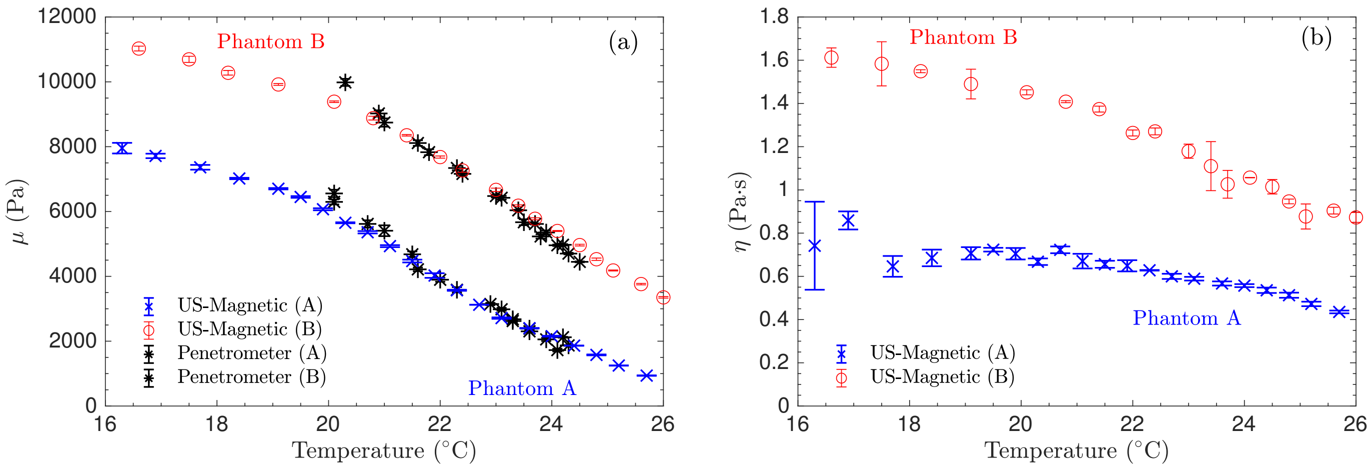

Fig. 5. Temperature-dependence of the shear elastic moduli. (a) Shear elastic modulus (μ) measured experimentally for phantom A (blue markers) and phantom B (red circles). The quasi-static elastic parameters measured using a flat-ended cylindrical indenter are shown in markers (asterisk). (b) Shear viscous modulus (η) measured experimentally at different temperatures for phantom A (blue markers) and phantom B (red circles).

measured showing negligible variations between repetitions. This is extremely important in this kind of materials because, as we will show in the next Section, shear elasticity in gelatins is strongly dependent on temperature.

C. Temperature dependence of viscoelastic properties

In order to test the robustness and consistency of the viscoelastic parameters estimated using the present method, a temperature dependence study was carried out. Using the viscoelastic phantoms A and B, a set of tests were performed while temperature was slowly increased from 16° C to 26° C, i.e., up to room temperature. First, the temperature-dependent viscoelastic parameters are shown in Figs. 5 (a, b). The estimated parameters are shown in blue (red) markers for phantom A (phantom B). On the one hand, for the real part of the shear modulus, shown in Fig. 5 (a), we observe that at low temperatures the experimental data asymptotically converges to a constant value. On the other hand, the gelatin becomes softer as the temperature rises, and the shear elastic modulus decreases. Note that at a temperature around 26° C the gelatin is about to reach a phase transition from soft-solid to viscous fluid and the method is no longer applicable.

Finally, the quasi-static viscoelastic parameters using the indentation tests are shown in Fig. 5 for both samples. The values obtained by penetrometry agree with those obtained by the proposed hybrid method for the range of measured temperatures. Both methods describe the softening of the gelatins as temperature increases and the values of elastic modulus are in good agreement.

V. Discussion and Conclusions

We propose a method to locally assess the complex shear modulus of a viscoelastic medium based on the measurement of the dynamical response of a millimetre-size ferromagnetic sphere embedded on it under the action of a known magnetic force. The magnetic force was produced with a classical magneto-motive ultrasound setup consisting of a coil and a ferritic steel core. Both, measured magnetic field and the magnetic forces acting on the ferromagnetic sphere agree with simulations and theory. Finally, the measured displacement of the sphere inside the phantom was fitted to an incompressible Kelvin-Voigt-type viscoelastic model to obtain the shear elastic and viscous coefficients.

Two kind of phantoms presenting different viscoelastic properties were considered: a) water and gelatin powder and b) water, gelatin powder and glycerin. Their mechanical properties were monitored as a function of the temperature, showing a decrease in both the shear elastic and the shear viscous coefficients when temperature increases. The shear elastic coefficient of the different phantoms was independently validated using a quasi-static indentation technique, showing good agreement between the results of the indentation test and the proposed method combining ultrasound and magnetic forces. The maximum error was estimated to be around 10% at low temperature, although errors remain well below 5% for most temperatures.

As the generated magnetic field rapidly decays with distance, the penetration depth is limited in the present setup to 1.5 or 2 cm. Note ARF-based techniques are able to focus ultrasound beams at several centimetres. However, as most soft-solids are weak diamagnetic, the present system allows a precise estimation of the force acting on the inclusion. If the distance from the sphere to the ferritic core is measured, this system improves the reliability of the force calculation with respect to the estimated force using acoustic radiation force techniques. Note the measurement of the location of the sphere can be accurately performed using the pulse-echo system. In ARF-based techniques, the force can vary due to a broad range of factors that include nonlinearities, inhomogeneities or attenuation in the path between the transducer and the sphere. In contrast, weak diamagnetic medium does not influence the value of the magnetic force. For this reason, the proposed technique allows a robust characterization of the medium, and is able to provide not only the elastic shear coefficient, but the viscous shear coefficient. Note that, as occurs with ARF-based techniques, the theory used here for the fitting assumes a homogeneous medium. If shear waves are scattered by an abrupt change of elastic properties or density, the particle vibration will be the superposition of the free oscillation and the motion due to reflected shear waves. Therefore, the method is restricted to homogeneous media. In particular, for soft-solids of shear modulus in the range 1 kPa to 10 kPa, a volume with a radius of 15 mm around the sphere should not create strong shear wave reflections.

It is worth to mention that MMUS imaging techniques using magnetic nanoparticles excited using an externally applied magnetic field and then imaged using ultrasound have been proposed in the past [18]–[22]. Using its pulsed modality these techniques allow the visualization of events at molecular and cellular levels [31], [32]. The potential of this technique to asses viscoelastic properties of tissues was also pointed out but specific values were not reported [33]. Moreover, MMUS systems have been used to generate shear acoustic waves for ultrasound elastography imaging [17], [34] or to generate pulsed displacements for optical coherence elastography [35]. MMUS techniques have been applied *in vivo* [36], [37], and they have been combined with other imaging techniques such as photoacoustics [38], PET or MRI [39]. In the proposed method, we employ a macroscopic ferromagnetic inclusion instead of using magnetic nanoparticles. Because of the size of the object, the in-vivo application of the method for tissue elastography is limited. However, due to the fact that the force and the induced displacements can be accurately described by analytical methods when using a macroscopic object, the proposed method results in an precise estimation of the viscoelastic parameters, which may have potential applications in viscoelastic material characterization in industry. In order to envision potential applications in the medical field using this technique, replace the macroscopic object with magnetic nanoparticles will be mandatory, which will result in a more complicated estimation of the magnetic force due to the unknown distribution of the nanoparticles within the tissue. However, effort has been made in the research community in order to precisely estimate the magnetic force while applying a magnetic field to magnetic nanoparticles [40], [41], making feasible to extend this technique to a more realistic preclinical/clinical application.

Acknowledgment

This research has been supported by the Spanish Ministry of Science, Innovation and Universities through grant "Juan de la Cierva - Incorporación" (IJC2018-037897-I), and program "Proyectos I+D+i 2019" (PID2019-111436RB-C22), by the Agència Valenciana de la Innovació through grant INNCON/2021/8 and by Generalitat Valenciana through grant AICO/2020/268. Action co-financed by the European Union through the Programa Operativo del Fondo Europeo de Desarrollo Regional (FEDER) of the Comunitat Valenciana 2014-2020 (IDIFEDER/2018/022). A.C. received financial support from Universitat Politècnica de València through program PAID-10-19. We thank Juan Pablo Rigla for his technical support with the magnetic field characterization.

References

[1] S. Aglyamov and A. Skovoroda, "Mechanical properties of soft biological tissues," *Biophysics*, vol. 45, no. 6, pp. 1103–1111, 2000.

[2] J. Ophir, S. K. Alam, B. S. Garra, F. Kallel, E. E. Konofagou, T. Krouskop, C. R. Merritt, R. Righetti, R. Souchon, S. Srinivasan *et al.*, "Elastography: imaging the elastic properties of soft tissues with ultrasound," *Journal of medical ultrasonics*, vol. 29, no. 4, p. 155, 2002.

[3] A. Sarvazyan, "Elastic properties of soft tissues," in *Handbook of Elastic Properties of Solids, Liquids, and Gases*, M. Levy, H. Bass, and R. Stern, Eds. New York: Academic Press, 2001, vol. 3, pp. 107–127.

[4] M. T. Shaw and W. J. MacKnight, *Introduction to polymer viscoelasticity*. John Wiley & Sons, 2005.

[5] E. Riande, R. Diaz-Calleja, M. Prolongo, R. Masegosa, and C. Salom, *Polymer viscoelasticity: stress and strain in practice*. CRC Press, 1999.

[6] L. Fan, L. Wong, and G. Ma, "Experimental investigation and modeling of viscoelastic behavior of concrete," *Construction and Building Materials*, vol. 48, pp. 814–821, 2013.

[7] L. Ferrari, J. Kaufmann, F. Winnefeld, and J. Plank, "Multi-method approach to study influence of superplasticizers on cement suspensions," *Cement and Concrete Research*, vol. 41, no. 10, pp. 1058–1066, 2011.

[8] S. Alam and F. Hammoum, "Viscoelastic properties of asphalt concrete using micromechanical self-consistent model," *Archives of Civil and Mechanical Engineering*, vol. 15, no. 1, pp. 272–285, 2015.

[9] B. McKenna and J. Lyng, "Introduction to food rheology and its measurement," *Texture in food*, vol. 1, pp. 130–160, 2003.

[10] N. Jimenez, R. Picó, F. Camarena, J. Redondo, and B. Roig, "Ultrasonic evaluation of the hydration degree of the orange peel," *Postharvest biology and technology*, vol. 67, pp. 130–137, 2012.

[11] H. L. Oestreicher, "Field and impedance of an oscillating sphere in a viscoelastic medium with an application to biophysics," *The Journal of the Acoustical Society of America*, vol. 23, no. 6, pp. 707–714, 1951.

[12] Y. A. Ilinskii, G. D. Meegan, E. A. Zabolotskaya, and S. Y. Emelianov, "Gas bubble and solid sphere motion in elastic media in response to acoustic radiation force," *The Journal of the Acoustical Society of America*, vol. 117, no. 4, pp. 2338–2346, 2005.

[13] S. R. Aglyamov, A. B. Karpiouk, Y. A. Ilinskii, E. A. Zabolotskaya, and S. Y. Emelianov, "Motion of a solid sphere in a viscoelastic medium in response to applied acoustic radiation force: Theoretical analysis and experimental verification," *The Journal of the Acoustical Society of America*, vol. 122, no. 4, pp. 1927–1936, 2007.

[14] M. W. Urban, I. Z. Nenadic, S. A. Mitchell, S. Chen, and J. F. Greenleaf, "Generalized response of a sphere embedded in a viscoelastic medium excited by an ultrasonic radiation force," *The Journal of the Acoustical Society of America*, vol. 130, no. 3, pp. 1133–1141, 2011.

[15] S. Chen, M. Fatemi, and J. F. Greenleaf, "Remote measurement of material properties from radiation force induced vibration of an embedded sphere," *The Journal of the Acoustical Society of America*, vol. 112, no. 3, pp. 884–889, 2002.

[16] A. B. Karpiouk, S. R. Aglyamov, Y. A. Ilinskii, E. A. Zabolotskaya, and S. Y. Emelianov, "Assessment of shear modulus of tissue using ultrasound radiation force acting on a spherical acoustic inhomogeneity," *IEEE transactions on ultrasonics, ferroelectrics, and frequency control*, vol. 56, no. 11, 2009.

[17] M. W. Urban, R. R. Kinnick, M. Mehrmohammadi, and J. F. Greenleaf, "Shear waves generated with magnetomotive force on an embedded sphere," in *2014 IEEE International Ultrasonics Symposium*. IEEE, 2014, pp. 723–726.

[18] J. Oh, M. D. Feldman, J. Kim, C. Condit, S. Emelianov, and T. E. Milner, "Detection of magnetic nanoparticles in tissue using magneto-motive ultrasound," *Nanotechnology*, vol. 17, no. 16, p. 4183, 2006.

[19] M. Mehrmohammadi, J. Oh, S. R. Aglyamov, A. B. Karpiouk, and S. Y. Emelianov, "Pulsed magneto-acoustic imaging," in *Engineering in Medicine and Biology Society, 2009. EMBC 2009. Annual International Conference of the IEEE*. IEEE, 2009, pp. 4771–4774.

[20] T. Z. Pavan, D. R. Sampaio, A. A. Carneiro, and D. T. Covas, "Ultrasound-based transient elastography using a magnetic excitation," in *Ultrasonics Symposium (IUS), 2012 IEEE International*. IEEE, 2012, pp. 1846–1849.

[21] M. Evertsson, M. Cinthio, S. Fredriksson, F. Olsson, H. W. Persson, and T. Jansson, "Frequency-and phase-sensitive magnetomotive ultrasound imaging of superparamagnetic iron oxide nanoparticles," *IEEE transactions on ultrasonics, ferroelectrics, and frequency control*, vol. 60, no. 3, pp. 481–491, 2013.

[22] A. G. Pope, G. Wu, F. Y. McWhorter, E. P. Merricks, T. C. Nichols, T. J. Czernuszewicz, C. M. Gallippi, and A. L. Oldenburg, "Contrast-

enhanced imaging of SPIO-labeled platelets using magnetomotive ultrasound," *Physics in Medicine & Biology*, vol. 58, no. 20, p. 7277, 2013.

[23] J. F. Schenck, "Safety of strong, static magnetic fields," *Journal of magnetic resonance imaging*, vol. 12, no. 1, pp. 2–19, 2000.

[24] ——, "The role of magnetic susceptibility in magnetic resonance imaging: Mri magnetic compatibility of the first and second kinds," *Medical physics*, vol. 23, no. 6, pp. 815–850, 1996.

[25] A. Mehdizadeh, R. Mei, J. F. Klausner, and N. Rahmatian, "Interaction forces between soft magnetic particles in uniform and non-uniform magnetic fields," *Acta Mechanica Sinica*, vol. 26, no. 6, pp. 921–929, 2010.

[26] D. A. DeAntonio, "Soft magnetic ferritic stainless steels," *Advanced materials & processes*, vol. 161, no. 10, pp. 29–32, 2003.

[27] R. Fitzpatrick, *Classical electromagnetism*, I. 978-1530325917, Ed. Createspace Independent Pub, 2016.

[28] M. A. Lubinski, S. Y. Emelianov, and M. O'Donnell, "Speckle tracking methods for ultrasonic elasticity imaging using short-time correlation," *IEEE transactions on ultrasonics, ferroelectrics, and frequency control*, vol. 46, no. 1, pp. 82–96, 1999.

[29] J. Harding and I. Sneddon, "The elastic stresses produced by the indentation of the plane surface of a semi-infinite elastic solid by a rigid punch," in *Mathematical Proceedings of the Cambridge Philosophical Society*, vol. 41, no. 1. Cambridge University Press, 1945, pp. 16–26.

[30] C. T. McKee, J. A. Last, P. Russell, and C. J. Murphy, "Indentation versus tensile measurements of young's modulus for soft biological tissues," *Tissue Engineering Part B: Reviews*, vol. 17, no. 3, pp. 155–164, 2011.

[31] M. Mehrmohammadi, K. Yoon, M. Qu, K. Johnston, and S. Emelianov, "Enhanced pulsed magneto-motive ultrasound imaging using superparamagnetic nanoclusters," *Nanotechnology*, vol. 22, no. 4, p. 045502, 2010.

[32] M. Mehrmohammadi, M. Qu, L. L. Ma, D. K. Romanovicz, K. P. Johnston, K. V. Sokolov, and S. Y. Emelianov, "Pulsed magneto-motive ultrasound imaging to detect intracellular accumulation of magnetic nanoparticles," *Nanotechnology*, vol. 22, no. 41, p. 415105, 2011.

[33] M. Mehrmohammadi, S. Aglyamov, A. Karpiouk, J. Oh, and S. Emelianov, "Pulsed magneto-motive ultrasound to assess viscoelastic properties of soft tissues," in *Proceedings of the Seventh International Conference on the Ultrasonic Measurement and Imaging of Tissue Elasticity*, vol. 106, 2008.

[34] T. W. Almeida, D. R. T. Sampaio, A. C. Bruno, T. Z. Pavan, and A. A. Carneiro, "Comparison between shear wave dispersion magneto motive ultrasound and transient elastography for measuring tissue-mimicking phantom viscoelasticity," *IEEE transactions on ultrasonics, ferroelectrics, and frequency control*, vol. 62, no. 12, pp. 2138–2145, 2015.

[35] V. Crecea, A. Ahmad, and S. A. Boppart, "Magnetomotive optical coherence elastography for microrheology of biological tissues," *Journal of biomedical optics*, vol. 18, no. 12, p. 121504, 2013.

[36] M. Evertsson, M. Cinthio, P. Kjellman, S. Fredriksson, R. Andersson, H. Toftevall, H. W. Persson, and T. Jansson, "In vivo magnetomotive ultrasound imaging of rat lymph nodes-a pilot study," in *Ultrasonics Symposium (IUS), 2015 IEEE International*. IEEE, 2015, pp. 1–4.

[37] A. C. Bruno, D. R. Sampaio, T. Z. Pavan, O. Baffa, and A. A. Carneiro, "A hybrid transducer to evaluate stomach emptying by ultrasound and susceptometric measurements: an in vivo feasibility study," *IEEE transactions on ultrasonics, ferroelectrics, and frequency control*, vol. 62, no. 7, pp. 1288–1294, 2015.

[38] M. Qu, S. Kim, M. Mehrmohammadi, S. Mallidi, P. Joshi, K. Homan, Y.-S. Chen, and S. Emelianov, "Combined photoacoustic and magneto-motive ultrasound imaging," in *Photons Plus Ultrasound: Imaging and Sensing 2010*, vol. 7564. International Society for Optics and Photonics, 2010, p. 756433.

[39] M. Evertsson, P. Kjellman, M. Cinthio, R. Andersson, T. A. Tran, G. Grafström, H. Toftevall, S. Fredriksson, C. Ingvar, S.-E. Strand *et al.*, "Combined magnetomotive ultrasound, PET/CT, and MR imaging of 68 Ga-labelled superparamagnetic iron oxide nanoparticles in rat sentinel lymph nodes in vivo," *Scientific Reports*, vol. 7, no. 1, p. 4824, 2017.

[40] S. R Aglyamov, A. B Karpiouk, M. Mehrmohammadi, S. Yoon, S. Kim, Y. A Ilinskii, E. A Zabolotskaya, and S. Y Emelianov, "Elasticity imaging and sensing using targeted motion: from macro to nano," *Current Medical Imaging*, vol. 8, no. 1, pp. 3–15, 2012.

[41] I. G. Lim, S. Park, and J. Oh, "Theoretical development of a magnetic force and an induced motion in elastic media for a magneto-motive technique," *Journal of the Korean Physical Society*, vol. 69, no. 4, pp. 461–471, 2016.